

# Controlled Exfoliation of MoS<sub>2</sub> Crystals into Trilayer Nanosheets

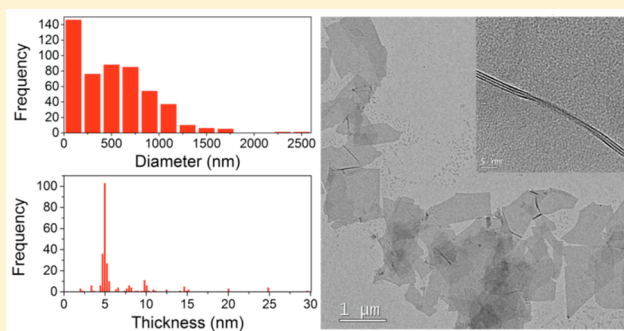
Xiaobin Fan,<sup>\*,†,‡</sup> Pengtao Xu,<sup>‡</sup> Yuguang C. Li,<sup>‡</sup> Dekai Zhou,<sup>‡</sup> Yifan Sun,<sup>‡</sup> Minh An T. Nguyen,<sup>‡</sup> Mauricio Terrones,<sup>‡</sup> and Thomas E. Mallouk<sup>\*,‡</sup>

<sup>†</sup>State Key Laboratory of Chemical Engineering, Collaborative Innovation Center of Chemical Science and Engineering, School of Chemical Engineering and Technology, Tianjin University, Tianjin 300072, China

<sup>‡</sup>Departments of Chemistry, Biochemistry and Molecular Biology, Physics, and Center for 2-Dimensional and Layered Materials, The Pennsylvania State University, University Park, Pennsylvania 16802, United States

## Supporting Information

**ABSTRACT:** The controlled exfoliation of transition metal dichalcogenides (TMDs) into pristine single- or few-layer nanosheets remains a significant barrier to fundamental studies and device applications of TMDs. Here we report a novel strategy for exfoliating crystalline MoS<sub>2</sub> into suspensions of nanosheets with retention of the semiconducting 2H phase. The controlled reaction of MoS<sub>2</sub> with substoichiometric amounts *n*-butyllithium results in intercalation of the edges of the crystals, which are then readily exfoliated in a 45 vol % ethanol–water solution. Surprisingly, the resulting colloidal suspension of nanosheets was found (by electron microscopy and atomic force microscopy) to consist mostly of trilayers. The efficiency of exfoliation of the pre-intercalated sample is increased by at least 1 order of magnitude relative to the starting MoS<sub>2</sub> microcrystals, with a mass yield of the dispersed nanosheets of 11–15%.



## INTRODUCTION

Layered materials have strong covalent bonds in plane and van der Waals bonding between sheets.<sup>1–4</sup> The weak interlayer bonding enables the exfoliation of these solids into two-dimensional nanosheets with electronic, mechanical, and catalytic properties that are not necessarily observed in their bulk counterparts.<sup>5–20</sup> Unlike micromechanical exfoliation, liquid-phase exfoliation enables the preparation of macroscopic quantities of exfoliated nanosheets for a variety of applications.<sup>21–26</sup> Over the past decade, significant advances have been achieved in the liquid phase exfoliation of graphite.<sup>27,28</sup> Many of these methods can be applied to other van der Waals solids such as transition-metal dichalcogenides (TMDs),<sup>22,29–33</sup> but some challenges still remain.

One crucial issue lies in the fact that the TMD sheets are three atom thick layers, with the transition metal atom sandwiched between two chalcogen layers. As a consequence, TMDs are polymorphic and can adopt structures with different electronic properties.<sup>34,35</sup> The archetypal example is MoS<sub>2</sub>, which in bulk form adopts a semiconducting hexagonal structure (2H phase) with trigonal prismatic coordination of Mo by S.<sup>36</sup> Unfortunately, the most efficient exfoliation route for MoS<sub>2</sub><sup>37–41</sup> involves the intercalation of guest species such as Li, which involves host–guest charge transfer.<sup>42</sup> Reduction can transform MoS<sub>2</sub> from the semiconducting 2H phase to the metallic 1T or 1T' phase, in which Mo is octahedrally coordinated.<sup>34</sup> A number of studies have shown that intercalation with lithium destabilizes the 2H phase of MoS<sub>2</sub>,

and a mixture of 1T and 2H phases is obtained in the exfoliated nanosheets.<sup>37,41,43</sup> Even though the 2H phase can be recovered after annealing<sup>37</sup> or infrared irradiation,<sup>43</sup> lattice distortions and vacancy defects are typically observed in the product.<sup>34</sup>

Direct exfoliation of MoS<sub>2</sub> crystals in solvents is a promising way to prepare high quality 2H MoS<sub>2</sub> nanosheets without these defects. As in the case of graphite,<sup>28</sup> the dispersive London interactions between MoS<sub>2</sub> layers can be compensated in a properly chosen solvent by minimizing the interfacial tension between the liquid and solid. Therefore, the exfoliation of MoS<sub>2</sub> crystals can proceed by ultrasonication<sup>44–47</sup> or shear mixing<sup>48</sup> in solvents with surface tension close to 40 mJ m<sup>−2</sup>. However, the yield of single- or few-layer (layer number  $N \leq 3$ ) nanosheets is low, and the sheets obtained have small lateral dimensions (<300 nm) and a broad range of  $N$ .<sup>46</sup> The best exfoliation results are achieved by using high-boiling organic solvents such as *N*-methyl-2-pyrrolidone (NMP) or surfactant solutions.<sup>28</sup> Recently, Vaia and co-workers have shown that the exfoliation yield in NMP is sensitive to trace water and dissolved oxygen.<sup>49</sup> They proposed a mechanism in which oxidation at edge plane sites facilitates the separation of sheets by polar solvents.

We reasoned that since the intercalation of layered materials is known to proceed from the edges of the crystal,<sup>50</sup> the edges might be more effectively activated for liquid phase exfoliation

Received: February 9, 2016

Published: March 31, 2016

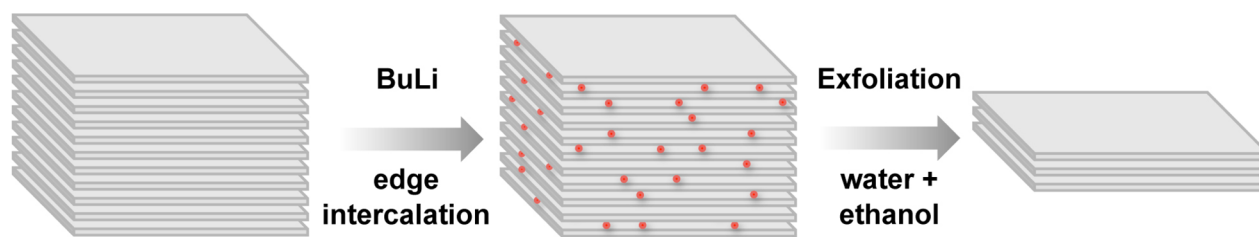


**Figure 1.** Illustration of the preparation of trilayer 2H MoS<sub>2</sub> by reaction with substoichiometric *n*-butyllithium followed by exfoliation in ethanol/water.

by using substoichiometric amounts of strong reducing agents that are known to intercalate MoS<sub>2</sub>. This idea is illustrated schematically in Figure 1. By varying the stoichiometry of *n*-butyllithium used in this process, we found that it is possible to avoid the 2H–1T phase change. Intercalation of Li into MoS<sub>2</sub> crystals at a 1/10 molar ratio results in efficient exfoliation in ethanol/water mixtures, to a mass yield of 11–15% exfoliated sheets. To our surprise, this process preferentially yields trilayer 2H MoS<sub>2</sub> nanosheets with lateral dimensions on the order of microns.

## RESULTS AND DISCUSSION

Bulk MoS<sub>2</sub> crystals were reacted with *n*-butyllithium in hexane at ambient temperature for 3 days. High-resolution X-ray photoelectron spectra (XPS) are consistent with earlier studies of electrochemical Li intercalation<sup>51</sup> and theoretical studies<sup>52</sup> and show the absence of the 1T phase when substoichiometric lithium ( $x = \text{Li}/\text{Mo} \leq 0.2$ ) is used (Figure 2). As the Li/Mo ratio is increased, the Mo 3d<sub>3/2</sub> and 3d<sub>5/2</sub> peaks gradually shift

to the lower binding energy, which can be attributed to the donation of electrons from intercalated Li to Mo. At higher Li/Mo ratios, both the Mo 3d<sub>3/2</sub> and 3d<sub>5/2</sub> peaks can be deconvoluted into two independent components with a separation of binding energy around 0.8 eV. This difference is consistent with a previous report<sup>51</sup> of the binding energies of the 2H and 1T MoS<sub>2</sub> phases.

The additional (001) and (002) peaks in the XRD for  $x > 0.1$  correspond to the Li<sub>*x-y*</sub>MoS<sub>2</sub>(H<sub>2</sub>O)<sub>*y*</sub> phase, which is formed by hydration of Li<sub>*x*</sub>MoS<sub>2</sub>. However, this compound does not necessarily adopt the 1T phase, as evidenced by XPS (Figure 2) and the results of DFT calculations (see Supporting Information). Li<sub>*x*</sub>MoS<sub>2</sub> can adopt the 2H phase for  $x > 0.2$ .

Structural changes in the MoS<sub>2</sub> crystals were further investigated by X-ray diffraction (XRD). In line with our recent report,<sup>43</sup> the intercalation of stoichiometric lithium ( $x = 1$ ) into MoS<sub>2</sub> slightly expands ( $\sim 0.15$  Å) the interlayer galleries. Hydration further shifts the (001) reflection to lower angle, as can be observed when the samples with  $x \geq 0.2$  are left open to the atmosphere (Figure 3). The intensity of the characteristic

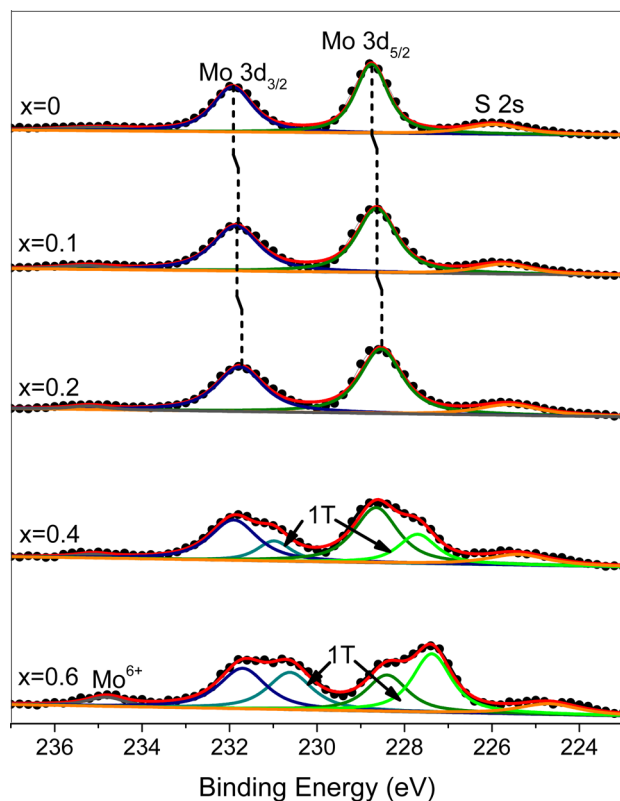


**Figure 2.** High-resolution XPS spectra of the MoS<sub>2</sub> crystals after reaction with different substoichiometric amounts ( $x = \text{Li}/\text{Mo}$ ) of *n*-butyllithium.

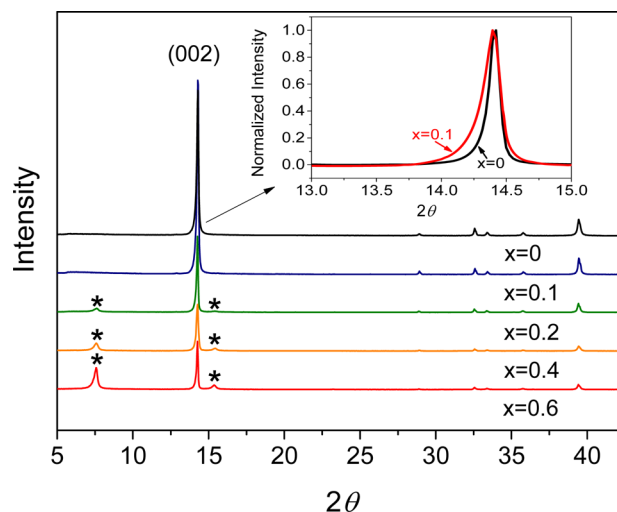


**Figure 3.** XRD patterns of MoS<sub>2</sub> crystals after reaction with different amounts of *n*-butyllithium. Additional (001) and (002) peaks (\*) of Li<sub>*x-y*</sub>MoS<sub>2</sub>(H<sub>2</sub>O)<sub>*y*</sub> emerge when  $x \geq 0.2$ , whereas only broadening of the (002) peak of 2H MoS<sub>2</sub> is observed when  $x = 0.1$  (inset). Note that Li<sub>*x-y*</sub>MoS<sub>2</sub>(H<sub>2</sub>O)<sub>*y*</sub> is not necessarily in the 1T phase.

peaks of hexagonal 2H MoS<sub>2</sub> rapidly decrease for  $x \geq 0.2$  because of the loss of long-range order that occurs when a mosaic of 2H and 1T phases is formed.<sup>34</sup> However, controlled reaction of MoS<sub>2</sub> with substoichiometric lithium ( $x = 0.1$ ) yields an XRD pattern that is nearly identical to that of the pristine crystals, except for slight broadening of the (002) peak

toward lower angles (inset), most likely due to the insertion of lithium at the edges of the MoS<sub>2</sub> sheets.

Based on these results, the Li<sub>0.1</sub>MoS<sub>2</sub> composition was chosen for exfoliation, with pristine MoS<sub>2</sub> as a control. Systematic studies of the exfoliation efficiency were carried out in a 45 vol % ethanol–water mixture, which has been shown to have reasonable exfoliation efficiency for TMDs.<sup>53</sup> Samples were sonicated in the mixed solvent with a horn sonicator. The resulting dispersions were centrifuged to remove any remaining bulk crystals, and the supernatant was decanted. *In situ* characterization of the diluted dispersions was carried out by UV–vis–NIR absorption spectroscopy.<sup>46</sup> Both the spectra of Li<sub>0.1</sub>MoS<sub>2</sub> and MoS<sub>2</sub> dispersions show the characteristic A and B transitions of exfoliated 2H MoS<sub>2</sub> after sonication for only 1 h, despite the great difference in their absorption intensity and curve shapes (Figure 4a). According to a recent

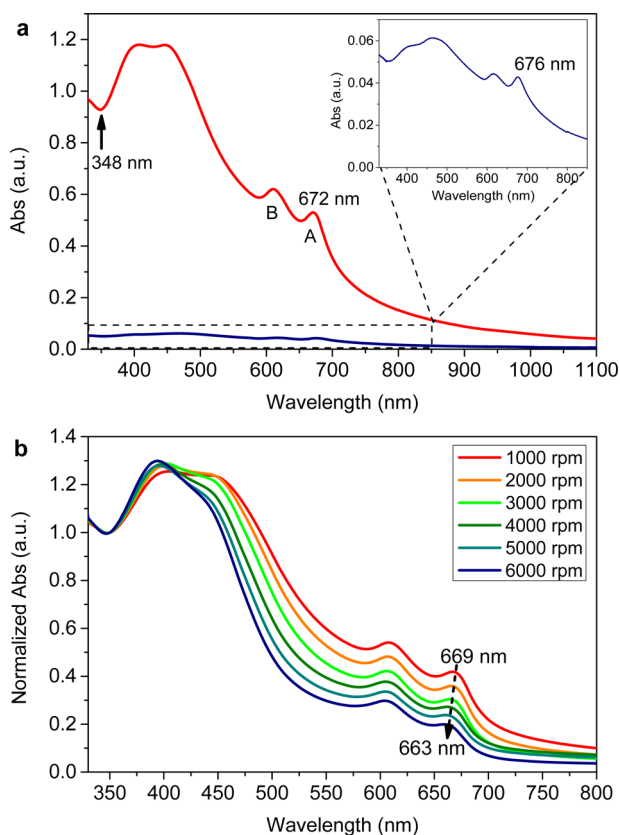


**Figure 4.** (a) UV–vis–NIR spectra of the Li<sub>0.1</sub>MoS<sub>2</sub> (red line) and MoS<sub>2</sub> (blue line) dispersions. The dispersions were diluted identically for comparison. The initial Li<sub>0.1</sub>MoS<sub>2</sub> or MoS<sub>2</sub> concentration was 7.5 mg mL<sup>-1</sup>, and sonication (40% × 700 W) was carried out for 1 h followed by standard centrifugation at 2000 rpm for 30 min. (b) UV–vis–NIR spectra of Li<sub>0.1</sub>MoS<sub>2</sub> dispersions obtained under optimized conditions. The spectra are normalized to the intensity at 348 nm. The initial Li<sub>0.1</sub>MoS<sub>2</sub> concentration was 15 mg mL<sup>-1</sup>, and sonication (40% × 700 W) was carried out for 2 h followed by centrifugation at 1000–6000 rpm for 30 min.

study by Coleman and co-workers,<sup>46</sup> the local minimal extinction at ~345 nm (348 nm in our case) rather than the A- or B-exciton should be used to estimate the concentration of exfoliated MoS<sub>2</sub>, given the scattering of nanosheets of different sizes and thicknesses. Repeated experiments and quantitative tests confirm that the two spectra show at least 1 order of magnitude difference in the extinction at 348 nm, suggesting a

significant increase in the concentration of MoS<sub>2</sub> nanosheets when Li<sub>0.1</sub>MoS<sub>2</sub> was used. Furthermore, the A-exciton peak of the Li<sub>0.1</sub>MoS<sub>2</sub> dispersion shows an obvious blue-shift of 4 nm relative to the MoS<sub>2</sub> control sample, indicating an increase in the optical band gap and thus a decrease in the average thickness of the nanosheets.<sup>54</sup>

To obtain the optimum parameters for the exfoliation, we systematically studied the sonication time, initial concentration, and centrifugation rate (see details in Supporting Information). Under optimized conditions (Experimental Section), a highly concentrated, dark green dispersion can be directly obtained after sonication for 2 h (see Supporting Information). The final dispersions were obtained after centrifugation at 1000–6000 rpm for 30 min, and their normalized UV–vis–NIR spectra are shown in Figure 4b. A continuous blue-shift of the A-exciton from 669 to 663 nm can be clearly observed after centrifugation at different speeds. According to a recent study, the average layer numbers ( $N_{\text{avg}}$ ) of exfoliated 2H MoS<sub>2</sub> nanosheets can be estimated from an empirical equation based on the A-exciton absorbance.<sup>46</sup> Considering that limited intercalation occurs in our experiments and the 2H structure is retained in the product, the product is chemically very similar to solvent-exfoliated MoS<sub>2</sub> and should have similar optical properties. Thus, the  $N_{\text{avg}}$  of MoS<sub>2</sub> nanosheets in the dispersions after centrifugation at 1000 to 6000 rpm can be estimated to be 5.4 to 2.6, respectively. Corresponding concentrations can be directly measured to be around 2.2 to 1.6 mg mL<sup>-1</sup> by vacuum drying methods, owing to the low-boiling-point nature of the ethanol–water mixture. These values are about 2 orders of magnitude greater than the highest reported concentration of MoS<sub>2</sub> in ethanol/water (0.018 mg mL<sup>-1</sup>)<sup>53</sup> and are also higher than those found in organic solvents such as NMP.<sup>44</sup> As the initial concentration of the crystals was 15 mg mL<sup>-1</sup>, the yield by weight<sup>55</sup> of the dispersed nanosheets can be calculated to be 11–15%. Considering the decrease of  $N_{\text{avg}}$  in the different dispersions, the calculated extinction coefficients at 348 nm significantly decrease from around 19 to 5.3 mL mg<sup>-1</sup> cm<sup>-1</sup>, probably due to the reduced scattering and increased transparency in the thinner nanosheets. This hypothesis is supported by the significantly reduced scattering background when compared with previous studies,<sup>44,56</sup> as well as the obviously reduced scattering background with increasing centrifugation speed (please see details in Supporting Information).

Despite the fact that calculated extinction coefficients may vary for different instruments and solvents, this interesting finding can explain, at least in part, the large deviation in reported extinction coefficients<sup>46</sup> (~69 mL mg<sup>-1</sup> cm<sup>-1</sup> at 345 nm) from previous studies, in which thicker nanosheets were involved. Normally, the thickness of MoS<sub>2</sub> nanosheets obtained by liquid exfoliation is always correlated with the lateral size of the sheets due to the greater interlayer binding energy associated with larger flakes. Therefore, single- or few-layer nanosheets with lateral sizes over 300 nm are rarely seen. However, this is not the case for exfoliation of Li<sub>0.1</sub>MoS<sub>2</sub>. As shown in Figure 5a–d, abundant nanosheets with lateral dimensions greater than 500 nm can be observed in the final dispersion (after centrifugation at 6000 rpm) by atomic force microscopy (AFM). To our surprise, most of these large nanosheets (~70%) with lateral sizes over 500 nm show the same apparent AFM height of ~5 nm (Figure 5e), although a few thinner or thicker nanosheets (multiples of ~5 nm in height) can be also found. A systematic analysis of the steps of

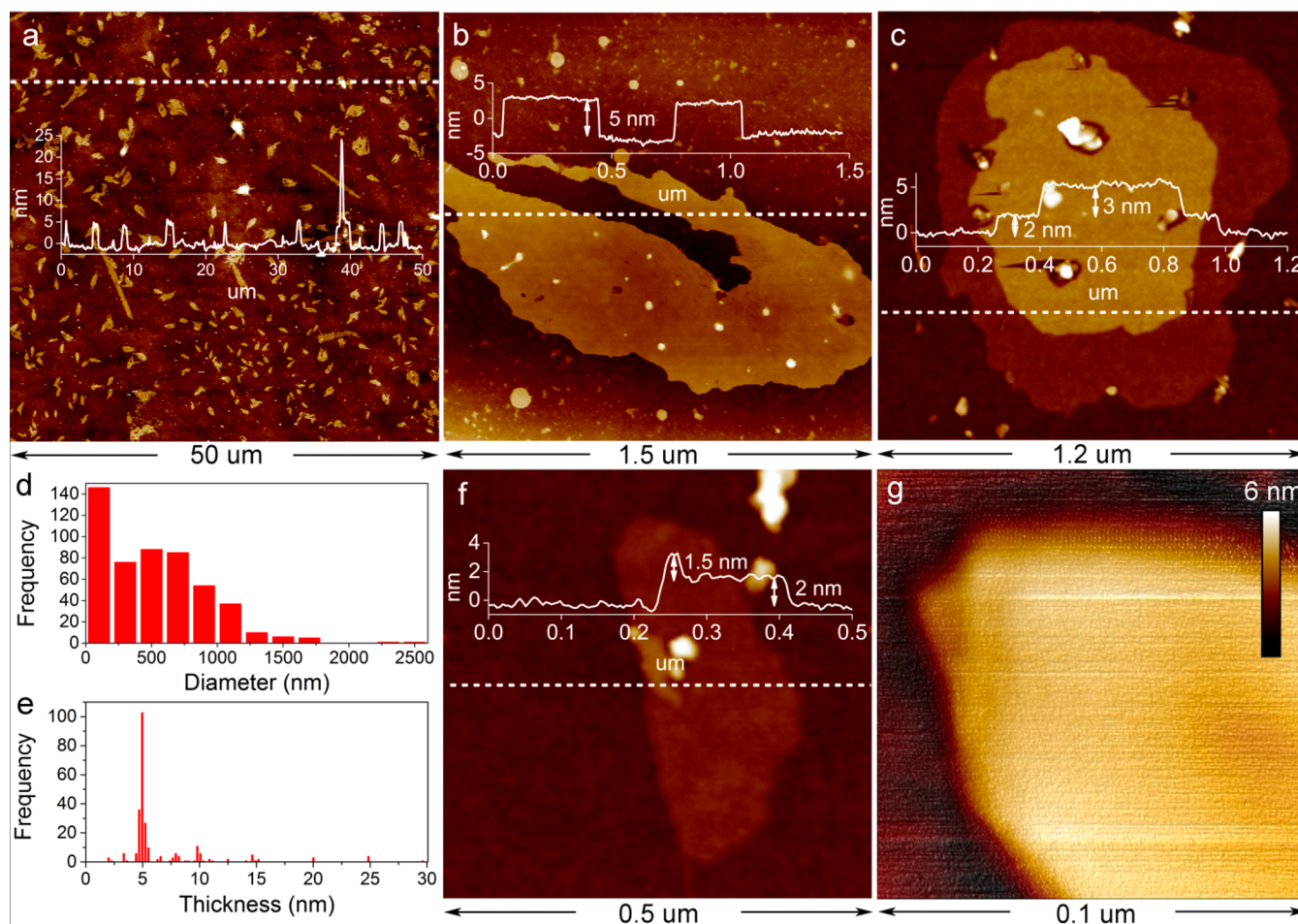


**Figure 5.** AFM images and the corresponding cross-sectional analysis of the exfoliated nanosheets. The lateral size distribution shown in (e) was counted from 509 nanosheets, and the thickness distribution is based on 261 nanosheets with lateral sizes over 500 nm (see more details in Supporting Information).

many nanosheets reveals that the apparent monolayer height is  $\sim 1.5$  nm (see additional step analysis in Supporting Information). The first step on the Si substrate is  $\sim 2$  nm (Figure 5f), and the difference likely arises from the weak sample/substrate interaction and the possible presence of trapped solvent.<sup>46</sup> These results suggest a trilayer structure for the vast majority of the exfoliated nanosheets, in agreement with the UV-vis-NIR results ( $N_{\text{avg}} = 2.56$ ). The trilayer structure can be directly observed for some nanosheets with clearly exposed edges (Figure 5g) and is further supported by high-resolution transmission electron microscopy (HRTEM) (Figure 6).

Nanosheets with lengths over  $1 \mu\text{m}$ , which are readily found by TEM, appear transparent and have uniform contrast (Figure 6a). The trilayer structure can be clearly observed in HRTEM images at the occasionally found folded edge (Figure 6b), with a parallel fringe spacing of  $0.673$  nm (see inset). This value is larger than that of bulk  $\text{MoS}_2$  ( $\sim 0.615$  nm), possibly due to the reduced interlayer binding energy.<sup>57</sup> Note that the interlayer distance here is obviously smaller than the apparent monolayer heights measured by AFM because of AFM instrumental offset (caused by different interaction forces) and the intrinsic out-of-plane deformation of two-dimensional structures.<sup>58</sup> The hexagonal lattice of 2H  $\text{MoS}_2$  is clearly visible in the basal plane by HRTEM (Figure 6c), representing the high degree of crystallinity of the  $\text{MoS}_2$  nanosheets. This conclusion is further

supported by the clear hexagonal selected area electron diffraction (SAED) pattern of the 2H structure (inset in Figure 6c). In scanning electron microscopy (SEM), it is easier to find the larger nanosheets with lengths over a few micrometers (Figure 6d,e). It should be noted that the SEM-based lateral size distribution (Figure 6f) is consistent with the AFM analysis, despite the potential to underestimate the number of small nanosheets owing to the difference in resolution of the two techniques.

The preferential exfoliation of  $\text{Li}_{0.1}\text{MoS}_2$  into large trilayer  $\text{MoS}_2$  nanosheets suggests the possibility that a staged intercalation compound should be formed in the reaction of bulk  $\text{MoS}_2$  crystals with substoichiometric amounts of *n*-butyllithium. Staging, in which guest species are inserted between every second layer, third layer, etc., is well-known for the intercalation of graphite.<sup>59</sup> In that case, the intercalation reaction always begins from a higher stage and progresses toward lower stages. However, only stage 1 compounds have been reported for lithium intercalation of TMDs,<sup>60</sup> despite the very long history of those intercalation reactions. Although XRD patterns (Figure 3) do not show evidence of staging, it is possible that such phases might not be detected if they formed only at the edges of the crystals. Therefore, we carried out density functional theory (DFT) calculations in order to estimate the relative stability of staged  $\text{Li}_x\text{MoS}_2$  compounds.

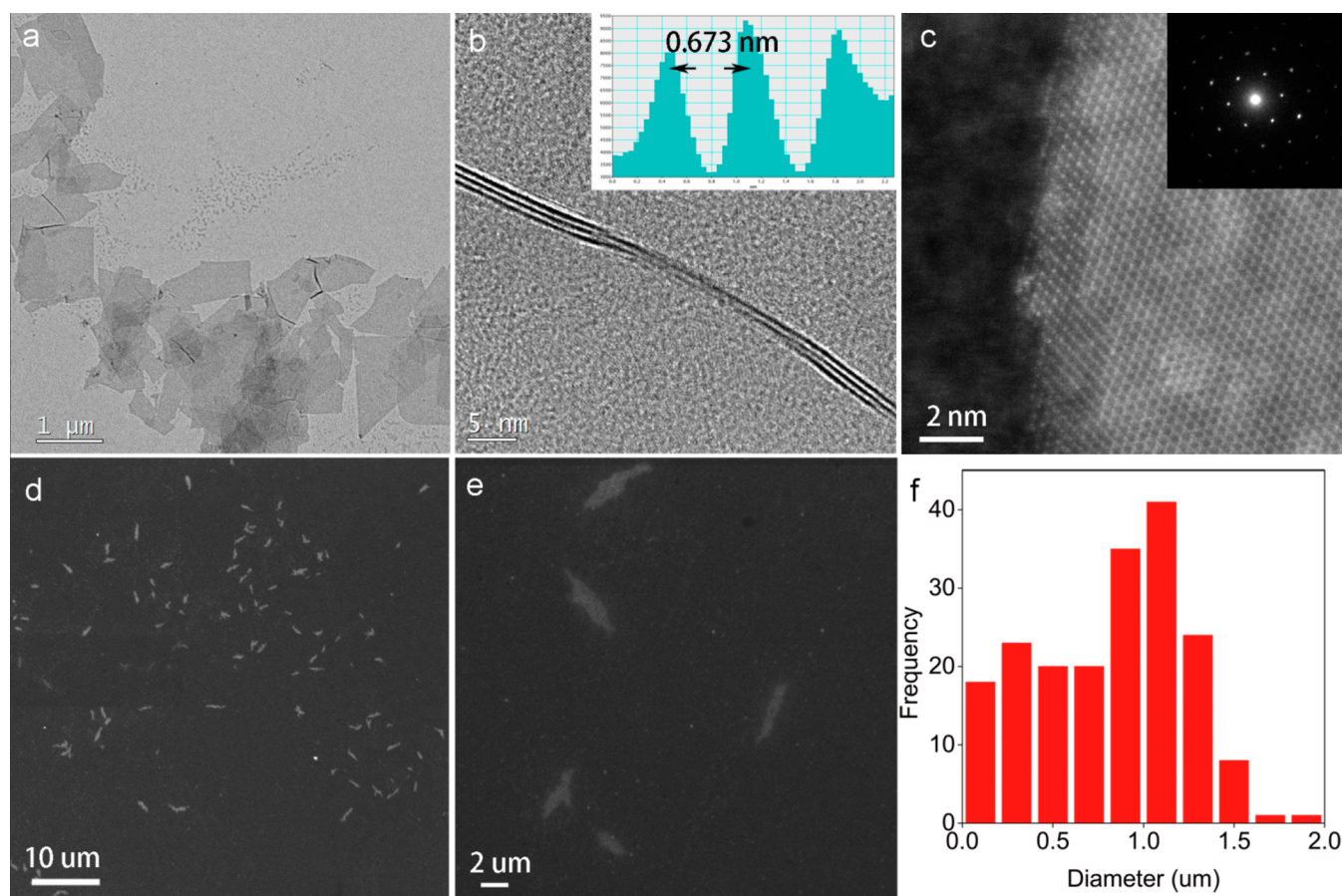


**Figure 6.** Representative TEM images of exfoliated MoS<sub>2</sub> nanosheets (a–c). SEM image of MoS<sub>2</sub> nanosheets on a Si substrate (d, e) and SEM-based size distribution counted from 191 nanosheets (f) (see [Supporting Information](#) for raw SEM data and additional details).

The results of the DFT calculations for various Li<sub>x</sub>MoS<sub>2</sub> structures are shown in [Figure 7](#). The calculated energies, on a per Li atom basis, of stage 1 and ordered higher stage compounds in the 2H structure are very similar, and therefore

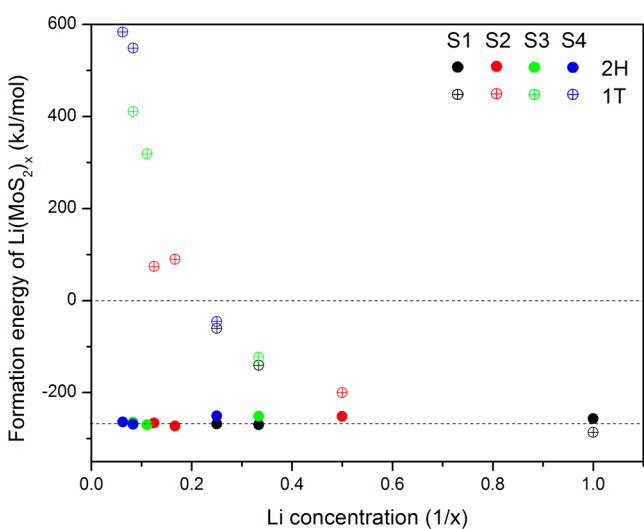


**Figure 7.** Formation energies (per mole of Li) of Li(MoS<sub>2</sub>)<sub>x</sub> calculated for different Li concentrations (1/x). S1, S2, S3, and S4 represent stage 1, stage 2, stage 3, and stage 4 structures, respectively. Filled and open circles represent 2H and 1T structures, respectively. Details of the DFT calculations are given in the [Supporting Information](#).

there is no strong support for the notion that a stage 3 compound, formed at the edges of the sheets, is the precursor to exfoliated trilayers. The calculations show nearly the same energy per Li atom for all structures in the 2H phase, but they indicate a clear energy difference between 1T and 2H structures, the latter being more stable at low Li/Mo ratios.

## CONCLUSION

In summary, we report a strategy for exfoliating MoS<sub>2</sub> crystals into trilayer 2H MoS<sub>2</sub> nanosheets, which cannot be produced selectively by other existing methods. Based on the experimental results and density functional theory calculations, the controlled reaction of MoS<sub>2</sub> with limited *n*-butyllithium results in partial intercalation without the undesirable 2H to 1T phase change. Intercalated lithium at the edge of the crystals may serve as a wedge to facilitate the exfoliation of MoS<sub>2</sub> by solvent molecules. Importantly, this method enables the preparation of nanosheets with controlled thickness and lateral dimensions in the micrometer range. The method described here may be applicable to the preparation of other exfoliated TMDs nanosheets with selective layer numbers, thus opening the possibility of producing layers on demand with desired electronic properties on a bulk scale.

## EXPERIMENTAL SECTION

**Controlled Intercalation and Exfoliation of MoS<sub>2</sub>.** The intercalation of MoS<sub>2</sub> was carried out by slowly reacting MoS<sub>2</sub> microcrystals (Acros Organics) with controlled amounts of *n*-butyllithium (1.6 M in hexane, Sigma-Aldrich) at room temperature.

For example, in order to obtain  $\text{Li}_{0.1}\text{MoS}_2$ , 4 g of  $\text{MoS}_2$  was stirred with 2.5 mmol *n*-butyllithium and 40 mL of hexanes in a 50 mL Schlenk flask under an  $\text{N}_2$  atmosphere at room temperature for 3 days. The resulting solid intercalated compound was washed with 30 mL of hexane three times and then dried under vacuum at room temperature. Note that for the intercalated dried samples ( $\text{Li}_x\text{MoS}_2$ ), some  $\text{Li}_{x-y}\text{MoS}_2(\text{H}_2\text{O})_y$  is formed when the samples are opened to the atmosphere, due to the irreversible hydration of  $\text{Li}_x\text{MoS}_2$ .

The dried pre-intercalated samples or bulk  $\text{MoS}_2$  crystals were exfoliated by sonication in an ethanol (45%)/water solution with a horn sonicator (QSONICA, Q700), followed by centrifugation (Eppendorf, model 5417C) to remove the remaining unexfoliated crystals. The optimized procedure for the preparation of trilayer  $\text{MoS}_2$  was 150 mg of dried  $\text{Li}_{0.1}\text{MoS}_2$  and 10 mL of ethanol/water loaded in a 20 mL vial, followed by sonication ( $40\% \times 700 \text{ W}$ ) for 2 h; the raw dispersion was centrifuged at 6000 rpm (3820g) for 30 min, and the top 2/3 of the supernatant was collected. For the UV–vis analysis, the raw dispersion ( $\sim 10 \text{ mL}$ ) after sonication was divided into equal portions for centrifugation at different speeds in order to provide parallel results for comparison. The concentration of  $\text{MoS}_2$  was calculated by repeatedly drying 1 mL of each dispersion on Al foil under vacuum, followed by measuring the weight difference with a microbalance (Sartorius, model SC2).

**Density Functional Theory Calculations.** All calculations were performed within the framework of density functional theory (DFT) as implemented in CASTEP.<sup>61</sup> The general gradient approximation (GGA) in the Perdew–Burke–Ernzerhof (PBE) form<sup>62</sup> was used to express the exchange–correlation energy. The van der Waals interaction between  $\text{MoS}_2$  layers was corrected using the semiempirical method proposed by Grimme.<sup>63,64</sup> The plane-waves basis with a cutoff energy of 350 eV and the conjugate gradient algorithm were applied to determine the electronic ground state with a convergence threshold of  $2.0 \times 10^{-6} \text{ eV/atom}$ . The tolerance for structural optimization was set at  $2.0 \times 10^{-5} \text{ eV/atom}$  for energy and  $0.05 \text{ eV/\AA}$  for force. The integrations over the Brillouin zone were performed by Monkhorst–Pack grids with a spacing of  $0.05 \text{ \AA}^{-1}$ . All calculations were spin polarized. Additional details can be found in the [Supporting Information](#).

**Characterization.** Samples were characterized by X-ray photoelectron spectroscopy (Kratos Analytical Axis Ultra), XRD (Philips Empyrean,  $\text{Cu K}\alpha$  radiation), UV–vis–NIR spectrophotometry (PerkinElmer Lambda 950), AFM (Bruker Icon microscope, peak force tapping mode), TEM (JEOL 1200 EXII), high-resolution TEM with SAED (FEI Titan3 G2), SEM (FEI NanoSEM 630 FESEM), and Raman spectroscopy (Renishaw inVia confocal microscope-based Raman spectrometer with 514.5 nm laser excitation).

## ■ ASSOCIATED CONTENT

### ● Supporting Information

The Supporting Information is available free of charge on the ACS Publications website at DOI: [10.1021/jacs.6b01502](https://doi.org/10.1021/jacs.6b01502).

Photograph of a concentrated nanosheet suspension, details of the determination of size and thickness distributions, additional Raman and UV–vis–NIR spectroscopic data, AFM data, and details of the DFT calculations ([PDF](#))

## ■ AUTHOR INFORMATION

### Corresponding Authors

\*E-mail [xiaobinfan@tju.edu.cn](mailto:xiaobinfan@tju.edu.cn) (X.F.).

\*E-mail [tem5@psu.edu](mailto:tem5@psu.edu) (T.E.M.).

### Notes

The authors declare no competing financial interest.

## ■ ACKNOWLEDGMENTS

This work is supported by the U.S. Army Research Office MURI Grant W911NF-11-1-0362. The authors acknowledge the Natural Science Funds for Excellent Young Scholars (No. 21222608) and the Program of Introducing Talents of Discipline to Universities (No. B06006). We thank Dr. Greg Barber and Danyun Xu for obtaining XPS spectra.

## ■ REFERENCES

- (1) Miro, P.; Audiffred, M.; Heine, T. *Chem. Soc. Rev.* **2014**, *43*, 6537.
- (2) Xu, M.; Liang, T.; Shi, M.; Chen, H. *Chem. Rev.* **2013**, *113*, 3766.
- (3) Rao, C. N. R.; Matte, H. S. S. R.; Maitra, U. *Angew. Chem., Int. Ed.* **2013**, *52*, 13162.
- (4) Nicolosi, V.; Chhowalla, M.; Kanatzidis, M. G.; Strano, M. S.; Coleman, J. N. *Science* **2013**, *340*, 1226419.
- (5) Yu, H. Y.; Liu, G. B.; Gong, P.; Xu, X. D.; Yao, W. *Nat. Commun.* **2014**, *5*, 3876.
- (6) Zhang, Y.; Chang, T. R.; Zhou, B.; Cui, Y. T.; Yan, H.; Liu, Z. K.; Schmitt, F.; Lee, J.; Moore, R.; Chen, Y. L.; Lin, H.; Jeng, H. T.; Mo, S. K.; Hussain, Z.; Bansil, A.; Shen, Z. X. *Nat. Nanotechnol.* **2013**, *9*, 111.
- (7) Allain, A.; Kang, J.; Banerjee, K.; Kis, A. *Nat. Mater.* **2015**, *14*, 1195.
- (8) Ross, J. S.; Wu, S. F.; Yu, H. Y.; Ghimire, N. J.; Jones, A. M.; Aivazian, G.; Yan, J. Q.; Mandrus, D. G.; Xiao, D.; Yao, W.; Xu, X. D. *Nat. Commun.* **2013**, *4*, 1474.
- (9) Seyler, K. L.; Schaibley, J. R.; Gong, P.; Rivera, P.; Jones, A. M.; Wu, S. F.; Yan, J. Q.; Mandrus, D. G.; Yao, W.; Xu, X. D. *Nat. Nanotechnol.* **2015**, *10*, 407.
- (10) Ross, J. S.; Klement, P.; Jones, A. M.; Ghimire, N. J.; Yan, J. Q.; Mandrus, D. G.; Taniguchi, T.; Watanabe, K.; Kitamura, K.; Yao, W.; Cobden, D. H.; Xu, X. D. *Nat. Nanotechnol.* **2014**, *9*, 268.
- (11) Zhu, W. J.; Low, T.; Lee, Y. H.; Wang, H.; Farmer, D. B.; Kong, J.; Xia, F. N.; Avouris, P. *Nat. Commun.* **2014**, *5*, 3087.
- (12) Wang, Q. H.; Kalantar-Zadeh, K.; Kis, A.; Coleman, J. N.; Strano, M. S. *Nat. Nanotechnol.* **2012**, *7*, 699.
- (13) Liu, K. H.; Zhang, L. M.; Cao, T.; Jin, C. H.; Qiu, D. A.; Zhou, Q.; Zettl, A.; Yang, P. D.; Louie, S. G.; Wang, F. *Nat. Commun.* **2014**, *5*, 4966.
- (14) Sangwan, V. K.; Jariwala, D.; Kim, I. S.; Chen, K. S.; Marks, T. J.; Lauhon, L. J.; Hersam, M. C. *Nat. Nanotechnol.* **2015**, *10*, 403.
- (15) Ugeda, M. M.; Bradley, A. J.; Shi, S. F.; da Jornada, F. H.; Zhang, Y.; Qiu, D. Y.; Ruan, W.; Mo, S. K.; Hussain, Z.; Shen, Z. X.; Wang, F.; Louie, S. G.; Crommie, M. F. *Nat. Mater.* **2014**, *13*, 1091.
- (16) Wang, X. M.; Jones, A. M.; Seyler, K. L.; Tran, V.; Jia, Y. C.; Zhao, H.; Wang, H.; Yang, L.; Xu, X. D.; Xia, F. N. *Nat. Nanotechnol.* **2015**, *10*, 517.
- (17) Scrace, T.; Tsai, Y.; Barman, B.; Schweidenback, L.; Petrou, A.; Kioseoglou, G.; Ozfidan, I.; Korkusinski, M.; Hawrylak, P. *Nat. Nanotechnol.* **2015**, *10*, 603.
- (18) Alidoust, N.; Bian, G.; Xu, S. Y.; Sankar, R.; Neupane, M.; Liu, C.; Belopolski, I.; Qu, D. X.; Denlinger, J. D.; Chou, F. C.; Hasan, M. Z. *Nat. Commun.* **2014**, *5*, 4673.
- (19) Qi, J. J.; Lan, Y. W.; Stieg, A. Z.; Chen, J. H.; Zhong, Y. L.; Li, L. J.; Chen, C. D.; Zhang, Y.; Wang, K. L. *Nat. Commun.* **2015**, *6*, 7430.
- (20) Hong, X. P.; Kim, J.; Shi, S. F.; Zhang, Y.; Jin, C. H.; Sun, Y. H.; Tongay, S.; Wu, J. Q.; Zhang, Y. F.; Wang, F. *Nat. Nanotechnol.* **2014**, *9*, 682.
- (21) Voiry, D.; Yamaguchi, H.; Li, J. W.; Silva, R.; Alves, D. C. B.; Fujita, T.; Chen, M. W.; Asefa, T.; Shenoy, V. B.; Eda, G.; Chhowalla, M. *Nat. Mater.* **2013**, *12*, 850.
- (22) Huang, X.; Zeng, Z.; Zhang, H. *Chem. Soc. Rev.* **2013**, *42*, 1934.
- (23) Acerce, M.; Voiry, D.; Chhowalla, M. *Nat. Nanotechnol.* **2015**, *10*, 313.
- (24) Yu, X. Y.; Prevot, M. S.; Guijarro, N.; Sivula, K. *Nat. Commun.* **2015**, *6*, 7596.
- (25) Chen, Y.; Tan, C.; Zhang, H.; Wang, L. *Chem. Soc. Rev.* **2015**, *44*, 2681.
- (26) Tan, C.; Zhang, H. *Chem. Soc. Rev.* **2015**, *44*, 2713.

- (27) Coleman, J. N. *Acc. Chem. Res.* **2013**, *46*, 14.
- (28) Ciesielski, A.; Samori, P. *Chem. Soc. Rev.* **2014**, *43*, 381.
- (29) Lv, R.; Robinson, J. A.; Schaak, R. E.; Sun, D.; Sun, Y. F.; Mallouk, T. E.; Terrones, M. *Acc. Chem. Res.* **2015**, *48*, 56.
- (30) Wang, H.; Yuan, H.; Hong, S. S.; Li, Y.; Cui, Y. *Chem. Soc. Rev.* **2015**, *44*, 2664.
- (31) Zeng, H.; Cui, X. *Chem. Soc. Rev.* **2015**, *44*, 2629.
- (32) Zhang, X.; Qiao, X.-F.; Shi, W.; Wu, J.-B.; Jiang, D.-S.; Tan, P.-H. *Chem. Soc. Rev.* **2015**, *44*, 2757.
- (33) Chhowalla, M.; Shin, H. S.; Eda, G.; Li, L. J.; Loh, K. P.; Zhang, H. *Nat. Chem.* **2013**, *5*, 263.
- (34) Voiry, D.; Mohite, A.; Chhowalla, M. *Chem. Soc. Rev.* **2015**, *44*, 2702.
- (35) Kuc, A.; Heine, T. *Chem. Soc. Rev.* **2015**, *44*, 2603.
- (36) Lin, Y. C.; Dumcencon, D. O.; Huang, Y. S.; Suenaga, K. *Nat. Nanotechnol.* **2014**, *9*, 391.
- (37) Eda, G.; Yamaguchi, H.; Voiry, D.; Fujita, T.; Chen, M. W.; Chhowalla, M. *Nano Lett.* **2011**, *11*, 5111.
- (38) Zheng, J.; Zhang, H.; Dong, S. H.; Liu, Y. P.; Nai, C. T.; Shin, H. S.; Jeong, H. Y.; Liu, B.; Loh, K. P. *Nat. Commun.* **2014**, *5*, 2995.
- (39) Eng, A. Y. S.; Ambrosi, A.; Sofer, Z.; Simek, P.; Pumera, M. *ACS Nano* **2014**, *8*, 12185.
- (40) Zeng, Z. Y.; Yin, Z. Y.; Huang, X.; Li, H.; He, Q. Y.; Lu, G.; Boey, F.; Zhang, H. *Angew. Chem., Int. Ed.* **2011**, *50*, 11093.
- (41) Knirsch, K. C.; Berner, N. C.; Nerl, H. C.; Cucinotta, C. S.; Gholamvand, Z.; McEvoy, N.; Wang, Z. X.; Abramovic, I.; Vecera, P.; Halik, M.; Sanvito, S.; Duesberg, G. S.; Nicolosi, V.; Hauke, F.; Hirsch, A.; Colernan, J. N.; Backes, C. *ACS Nano* **2015**, *9*, 6018.
- (42) Cheng, Y. C.; Nie, A. M.; Zhang, Q. Y.; Gan, L. Y.; Shahbazian-Yassar, R.; Schwingenschlogl, U. *ACS Nano* **2014**, *8*, 11447.
- (43) Fan, X. B.; Xu, P. T.; Zhou, D. K.; Sun, Y. F.; Li, Y. G. C.; Nguyen, M. A. T.; Terrones, M.; Mallouk, T. E. *Nano Lett.* **2015**, *15*, 5956.
- (44) Coleman, J. N.; Lotya, M.; O'Neill, A.; Bergin, S. D.; King, P. J.; Khan, U.; Young, K.; Gaucher, A.; De, S.; Smith, R. J.; Shvets, I. V.; Arora, S. K.; Stanton, G.; Kim, H. Y.; Lee, K.; Kim, G. T.; Duesberg, G. S.; Hallam, T.; Boland, J. J.; Wang, J. J.; Donegan, J. F.; Grunlan, J. C.; Moriarty, G.; Shmeliov, A.; Nicholls, R. J.; Perkins, J. M.; Grieveson, E. M.; Theuvsissen, K.; McComb, D. W.; Nellist, P. D.; Nicolosi, V. *Science* **2011**, *331*, 568.
- (45) Guan, G. J.; Zhang, S. Y.; Liu, S. H.; Cai, Y. Q.; Low, M.; Teng, C. P.; Phang, I. Y.; Cheng, Y.; Duei, K. L.; Srinivasan, B. M.; Zheng, Y. G.; Zhang, Y. W.; Han, M. Y. *J. Am. Chem. Soc.* **2015**, *137*, 6152.
- (46) Backes, C.; Smith, R. J.; McEvoy, N.; Berner, N. C.; McCloskey, D.; Nerl, H. C.; O'Neill, A.; King, P. J.; Higgins, T.; Hanlon, D.; Scheuschner, N.; Maultzsch, J.; Houben, L.; Duesberg, G. S.; Donegan, J. F.; Nicolosi, V.; Coleman, J. N. *Nat. Commun.* **2014**, *5*, 4576.
- (47) Jeong, S.; Yoo, D.; Ahn, M.; Miro, P.; Heine, T.; Cheon, J. *Nat. Commun.* **2015**, *6*, 5763.
- (48) Paton, K. R.; Varrla, E.; Backes, C.; Smith, R. J.; Khan, U.; O'Neill, A.; Boland, C.; Lotya, M.; Istrate, O. M.; King, P.; Higgins, T.; Barwich, S.; May, P.; Puczkarski, P.; Ahmed, I.; Moebius, M.; Pettersson, H.; Long, E.; Coelho, J.; O'Brien, S. E.; McGuire, E. K.; Sanchez, B. M.; Duesberg, G. S.; McEvoy, N.; Pennycook, T. J.; Downing, C.; Crossley, A.; Nicolosi, V.; Coleman, J. N. *Nat. Mater.* **2014**, *13*, 624.
- (49) Jawaid, A.; Nepal, D.; Park, K.; Jespersen, M.; Qualley, A.; Mirau, P.; Drummy, L. F.; Vaia, R. A. *Chem. Mater.* **2016**, *28*, 337.
- (50) Kovtyukhova, N. I.; Wang, Y. X.; Berkdemir, A.; Cruz-Silva, R.; Terrones, M.; Crespi, V. H.; Mallouk, T. E. *Nat. Chem.* **2014**, *6*, 957.
- (51) Wang, H. T.; Lu, Z. Y.; Xu, S. C.; Kong, D. S.; Cha, J. J.; Zheng, G. Y.; Hsu, P. C.; Yan, K.; Bradshaw, D.; Prinz, F. B.; Cui, Y. *Proc. Natl. Acad. Sci. U. S. A.* **2013**, *110*, 19701.
- (52) Enyashin, A. N.; Seifert, G. *Comput. Theor. Chem.* **2012**, *999*, 13.
- (53) Zhou, K. G.; Mao, N. N.; Wang, H. X.; Peng, Y.; Zhang, H. L. *Angew. Chem., Int. Ed.* **2011**, *50*, 10839.
- (54) Mak, K. F.; Lee, C.; Hone, J.; Shan, J.; Heinzl, T. F. *Phys. Rev. Lett.* **2010**, *105*, 136805.
- (55) Bonaccorso, F.; Lombardo, A.; Hasan, T.; Sun, Z.; Colombo, L.; Ferrari, A. C. *Mater. Today* **2012**, *15*, 564.
- (56) Smith, R. J.; King, P. J.; Lotya, M.; Wirtz, C.; Khan, U.; De, S.; O'Neill, A.; Duesberg, G. S.; Grunlan, J. C.; Moriarty, G.; Chen, J.; Wang, J.; Minett, A. I.; Nicolosi, V.; Coleman, J. N. *Adv. Mater.* **2011**, *23*, 3944.
- (57) Hu, Z.; Wang, L.; Zhang, K.; Wang, J.; Cheng, F.; Tao, Z.; Chen, J. *Angew. Chem., Int. Ed.* **2014**, *53*, 12794.
- (58) Brivio, J.; Alexander, D. T. L.; Kis, A. *Nano Lett.* **2011**, *11*, 5148.
- (59) Dresselhaus, M. S. *MRS Bull.* **1987**, *12*, 24.
- (60) Benavente, E.; Santa Ana, M. A.; Mendizabal, F.; Gonzalez, G. *Coord. Chem. Rev.* **2002**, *224*, 87.
- (61) Clark, S. J.; Segall, M. D.; Pickard, C. J.; Hasnip, P. J.; Probert, M. J.; Refson, K.; Payne, M. C. Z. *Kristallogr. - Cryst. Mater.* **2005**, *220*, 567.
- (62) Perdew, J. P.; Burke, K.; Ernzerhof, M. *Phys. Rev. Lett.* **1996**, *77*, 3865.
- (63) McNellis, E. R.; Meyer, J.; Reuter, K. *Phys. Rev. B: Condens. Matter Mater. Phys.* **2009**, *80*, 205414.
- (64) Grimme, S. *J. Comput. Chem.* **2006**, *27*, 1787.